

Fig. 4. Reflectance change at a wavelength of 1.5 μm ; inset shows the DBR peak shift versus the acetone molar fraction.

ily connected to an optical fiber obtaining a FOS with a working wavelength of 1.5 μm . On the other hand, the sensing element is widely tailorable, in the sense that one could explore other DBR parameters and metal nanoparticles in order to control the selectivity of the sensing element in different wavelength domains. The underlying physical phenomenon, i.e., the diffusion of solvent molecules in a metal nanoparticle/polymer composite layer, is indeed poorly understood and depends on several factors, such as the physical and chemical properties of the polymer and the metal nanoparticles.

In conclusion, the DBR based on Teflon-like and Au nanoparticle/Teflon-like polymers is a promising sensing element, the attraction of which is essentially threefold: first, the Teflon-like polymer is characterized by important properties such as a remarkable chemical resistance, a high thermal stability, a good flame resistance, and an excellent toughness, which are added to the typical polymer advantages such as low-cost fabrication and immense tailorability; second, the DBR can be easily integrated with an optical fiber, with the possibility of tuning the operation wavelength in the optical telecommunication range; third, the sensor can operate at room temperature. All these properties make this sensor particularly suitable for commercial devices, as well as for use in hostile conditions.

Experimental

DBR Deposition: The DBR was fabricated by an ion-beam sputtering technique at room temperature. This consisted of four pairs of Teflon-like (315 nm) and Au nanoparticle/Teflon-like composite (244 nm) on a Si substrate. The Teflon-like layers were deposited by sputtering a target of Teflon with an argon ion beam (Ar^+) with an energy of 850 eV and a current of 50 mA. The Au nanoparticle/Teflon-like composite layers were obtained by co-sputtering a target of Teflon and a target of Au using Ar^+ ion beams. The ion-beam sputtering the

Teflon target was characterized by an energy and a current fixed at 850 eV and 50 mA, respectively. The energy and the current of the ion-beam sputtering the Au target were 500 eV and 40 mA, respectively. The Au content in the Teflon-like composite layers was controlled by the deposition rates of the Au and Teflon species and checked by X-ray photoelectron spectroscopy (XPS) on reference samples. More details on the ion-beam sputtering deposition, and the structural and chemical properties of the Au nanoparticle/Teflon-like composite are reported elsewhere [16].

Vapor-Sensing Properties: The effects of the surrounding vapor on our sensing DBR were tested by reflectance measurements using a spectrophotometer arranged for experiments in the presence of gas or vapors. The samples were inserted into a glass tube through which flowed synthetic air (20.5 vol.-% O_2 in N_2) as carrier gas. The organic vapor was introduced by bubbling synthetic air through the organic liquid and the mixing the saturated synthetic air with the carrier gas to produce the desired concentration. The measurements were carried out at room temperature.

Received: December 19, 2002
Final version: March 24, 2003

- [1] K. T. V. Grattan, T. Sun, *Sens. Actuators A* **2000**, *82*, 40.
- [2] A. Convertino, A. Valentini, T. Ligonzo, R. Cingolani, *Appl. Phys. Lett.* **1997**, *71*, 732.
- [3] A. Convertino, A. Valentini, R. Cingolani, *Appl. Phys. Lett.* **1999**, *75*, 732.
- [4] P. K. H. Ho, D. S. Thomas, R. H. Friend, N. Tessler, *Science* **1999**, *285*, 233.
- [5] T. Vossmeier, B. Guse, I. Besnard, R. E. Bauer, K. Mullen, A. Yasuda, *Adv. Mater.* **1998**, *3*, 238.
- [6] G. Yu, J. Wang, J. McElvain, A. J. Heeger, *Adv. Mater.* **1998**, *10*, 1431.
- [7] P. J. Flory, *Principles of Polymer Chemistry*, Cornell University Press, Ithaca, New York **1953**.
- [8] L. R. G. Treolar, *The Physics of Rubber Elasticity*, Oxford University Press, Oxford **1975**.
- [9] a) T. Tanaka, S. T. Sun, Y. Hirokawa, S. Katayama, J. Kucera, Y. Hirose, T. Amiya, *Nature* **1987**, *325*, 796. b) T. Tanaka, D. Fillmore, S. T. Sun, I. Nishio, G. Swislo, A. Shah, *Phys. Rev. Lett.* **1980**, *45*, 1636.
- [10] R. J. Young, P. A. Lovell, *Introduction to Polymers*, Chapman and Hall, London **1981**.
- [11] F. A. Escobedo, J. J. de Pablo, *Phys. Rep.* **1999**, *318*, 85.
- [12] F. J. Doyle, *Responsive Gels, Volume Transitions*, Advances in Polymer Science, Vol. 1,2, Springer, Berlin **1993**.
- [13] K. Haraguchi, T. Takehisa, *Adv. Mater.* **2002**, *14*, 1120.
- [14] J. Perrin, B. Despax, E. Kay, *Phys. Rev. B* **1985**, *32*, 719.
- [15] J. Perrin, B. Despax, V. Hancett, E. Kay, *J. Vac. Sci. Technol. A* **1986**, *4*, 46.
- [16] A. Convertino, A. Valentini, A. Bassi, N. Cioffi, L. Torsi, E. N. M. Cirillo, *Appl. Phys. Lett.* **2002**, *80*, 1565.
- [17] M. Born, E. Wolf, *Principles of Optics*, Pergamon, New York **1964**.

Direction-Selective and Length-Tunable In-Plane Growth of Carbon Nanotubes**

By Anyuan Cao, Rajashree Baskaran, Matthew J. Frederick, Kimberly Turner, Pulickel M. Ajayan, and Ganapathiraman Ramanath*

Carbon nanotubes (CNTs) are fascinating one-dimensional molecular structures that can be either metallic or semiconducting, depending on their diameter and helicity.^[1–3] In order

[*] Prof. G. Ramanath, Dr. A. Cao, M. J. Frederick, Prof. P. M. Ajayan
Materials Science and Engineering Department
Rensselaer Polytechnic Institute
110 Eighth Street, Troy, NY 12180 (USA)
E-mail: ramanath@rpi.edu

R. Baskaran, Prof. K. Turner
Department of Mechanical and Environmental Engineering
University of California
Santa Barbara, CA 93106 (USA)

[**] The authors gratefully acknowledge funding from the Office of Naval Research under Grant No. N00014-00-1-0250, and GR's NSF CAREER Award DMR 9984478.

to create microelectronic devices comprised of CNT units, it is imperative to controllably place nanotubes in predefined orientations and configurations, and interconnect them both to each other and to other materials such as metal electrodes. Several methods have been suggested for controlled placement of CNTs onto electrode pairs, including alternating current (AC) bias-enhanced deposition^[4] and chemically modified adsorption.^[5] Direct growth of CNTs between pre-patterned electrodes by chemical vapor deposition (CVD) is a promising approach, since CVD growth is scalable and can be adapted to produce large-area CNT–electrode arrays.

While growth of *vertically* aligned CNTs on planar substrates by CVD has been reported extensively,^[6–9] obtaining nanotubes that are exclusively oriented *parallel* to the substrate in pre-determined orientations has been more difficult. Suspended CNTs across elevated structures have been produced recently, either by adjusting the gas flow^[10–12] or by applying an electrical field^[13,14] during CVD. However, both these approaches require pre-patterning of nanoscale catalyst particle assemblies. Also, the probability of nanotubes bridging across different catalyst islands is difficult to predict and control.

More recently, we reported a CVD-growth strategy to selectively grow unidirectionally oriented nanotubes on silica surfaces, in exclusion to silicon.^[15] We have combined this substrate selectivity with lithographic chiseling of SiO₂ layers to produce three-dimensional CNT architectures.^[16] Here, we adapt this methodology to exclusively grow CNT bundles in controlled directions parallel to the surface, by inhibiting CNT growth from certain SiO₂ pattern surfaces (e.g., the top surface) by covering them with a Au layer.^[17] The lengths of CNTs growing in different directions can be tuned by adjusting the Au coverage on respective SiO₂ pattern surfaces, the deposition time, and the SiO₂ pattern spacings. We utilize this strategy to fabricate arrays of low-electrical resistance nanotube–metal contact structures that could be attractive for creating nanotube-based electrical devices. The procedures used to prepare the SiO₂ patterns, and selectively cover certain portions with a Au layer, are described in the Experimental section and illustrated schematically in Figure 1.

We first describe the growth behavior of CNTs on pristine substrates, i.e., those that were not coated with Au before CVD. Figure 2a shows a representative scanning electronic microscopy (SEM) image of CNT architectures grown on a substrate with a row of SiO₂ patterns. We can see that nanotubes grow from all five surfaces of these patterns, i.e., the top surface and four sidewalls, forming a star-like structure (see inset of Fig. 2a). The CNTs in each direction are well aligned, and have the same length of ~25 μm. CNTs growing in opposite directions, towards each other between patterns cease to grow when they meet each other and form CNT–CNT interfaces (see arrow in Fig. 2b).

In contrast, CVD results on selectively Au-coated substrates show exclusive in-plane growth of aligned CNT bundles on SiO₂ surfaces that are not covered by Au. This is seen in Figure 2c, which shows 50 μm long CNT bridges grown

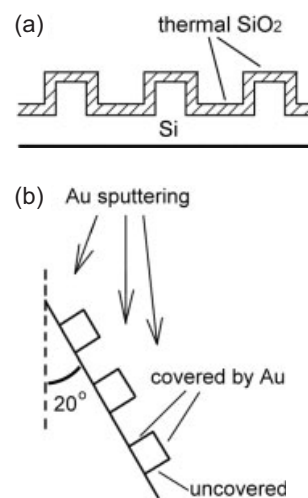


Fig. 1. Schematic illustrations of a) substrates with thermally-oxidized SiO₂ relief patterns, and b) their near-vertical placement during Au sputtering to selectively cover the top surface and the sidewall surfaces of the SiO₂ patterns that face the Au flux.

from the left sidewalls of SiO₂ patterns whose top and right sidewall surfaces are coated with Au. The CNTs grow straight, in a direction perpendicular to the silica surface seeding them, until they arrive at the next pattern (Fig. 2d). We note that the CNT growth terminates abruptly when the nanotube tips reach the sidewall of the next pattern, which serves as a barrier to further growth. This feature is seen in Figure 2e which shows a sharp interface between CNT tips and the pattern sidewall (covered by Au) where CNT growth stops.

The process of selectively coating Au on different SiO₂ surfaces can be harnessed to controllably grow CNTs along any sets of in-plane directions. For example, the nanotube growth direction was reversed by coating Au on the top surface and left sidewall of each pattern (Fig. 2f), in contrast to those shown in Figure 2c. We note that the CNT length is solely controlled by deposition time in the absence of physical obstacles in the growth direction. The CNTs grown from the last pattern of the row are ~80 μm long, while those grown between patterns are only 50 μm long, identical to the inter-pattern distance. This is a useful attribute in order to simultaneously bridge patterns with different inter-pattern distances by a single CVD process, where the growth time can be chosen to allow CNTs to bridge the longest inter-pattern gaps. Figures 2c,f also show that CNTs grown on the two sidewalls of SiO₂ patterns (indicated by two tilted arrows in Fig. 2f) are curled and shorter compared to the straight nanotube bundles between patterns. This result suggests that a lower Au coverage—due to line-of-sight Au flux during sputter-deposition—on these SiO₂ surfaces leads to short nanotubes with less alignment.

In order to examine this correlation, we measured the length of CNTs grown on SiO₂ surfaces with different Au coverages—measured by Rutherford backscattering spectrometry (RBS)—between 0 and 1.1×10^{17} atoms cm⁻². Our results show that CNT lengths decrease monotonically with increas-

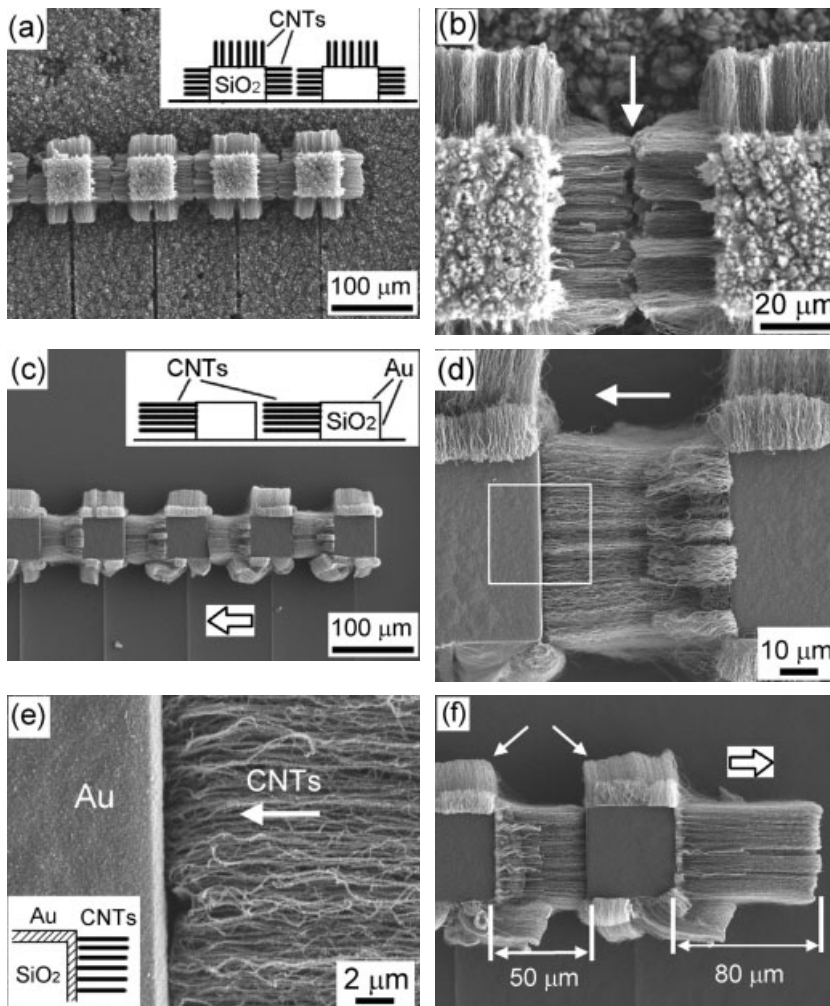


Fig. 2. a) Star-like growth of aligned CNTs on SiO₂ patterns without Au coverage. Inset shows a schematic sketch of the morphology. b) A high magnification view of (a) showing the CNT-CNT interface (see arrow) between SiO₂ patterns. c) Exclusive in-plane CNT growth from SiO₂ patterns obtained by selective Au sputtering on the top and right SiO₂ pattern surfaces (see inset), forming continuous nanotube bridges across a row of patterns. d) Enlarged view of aligned CNTs bridging two SiO₂ patterns. e) Close-up view of the highlighted area in (d), showing CNT-Au/SiO₂ interface where CNT growth stops; inset is a schematic illustration of the side-view of this interface; the hatched region shows the Au layer. f) CNT bridges having an opposite growth direction with respect to those shown in (c), obtained by coating Au on the top and left surfaces of the SiO₂ patterns. Note the larger length of the CNTs growing from the right face of the far right pillar. Tilted arrows show short and curled CNTs grown from other pattern surfaces. Horizontal arrows in (c), (d), (e), (f) indicate the CNT growth direction.

ing Au atom coverage (Fig. 3a), and no nanotube growth is observed for Au coverages above 1.1×10^{17} atoms cm⁻² (nominal thickness ~ 20 nm). While the actual mechanism of this decrease in CNT lengths is yet to be identified, the salient features of the nanotube growth process can be understood as follows. The as-deposited Au layer on SiO₂ transforms into islands of sizes between a few tens and a few hundreds of nanometers upon annealing to the CVD temperature of ~ 800 °C (Fig. 3b). In contrast, the as-deposited Au layers prior to annealing are continuous films, with no observable surface features at this length scale. Based on these results, we propose that the Au islands decrease the intake and interac-

tions of carbon/catalyst flux with SiO₂, leading to a decrease in the nanotube growth rate. This results in decreased CNT lengths, with increasing Au coverage for a given deposition time. For Au coverages greater than $\sim 1.1 \times 10^{17}$ atoms cm⁻², the Au layer remains continuous during CVD and masks the entire SiO₂ surface, thus completely preventing CNT growth. The CNT length dependence on the Au coverage is useful for obtaining CNTs of tunable lengths along different directions through control of Au coverage on different faces of SiO₂ patterns. This is illustrated in Fig. 3c, which shows CNTs of two different lengths growing from sidewalls that have been exposed to different Au fluxes through control of sample tilt during Au sputter deposition.

We carried out electrical resistance measurements with a two-point probe on Au coated SiO₂ patterns with and without CNT bridges to explore their use in mesoscale circuits. Figures 4a,b show a schematic sketch of the measurement geometry and plots of electrical resistance as a function of number of SiO₂ patterns, respectively. For all the three samples, the resistance increases linearly with the number of patterns. The circuit contact resistance between the probe and the Au layer on top of SiO₂ patterns ($= 2R_{\text{probe-Au}}$), obtained from the ordinate intercept of each plot, is also nearly constant at ~ 200 – 300 Ω for all samples. However, the average resistance between two adjacent patterns, denoted by the slope of the plots, is more than a factor of two smaller for patterns bridged by CNTs ($R_{\text{bridged}} = 54 \pm 2$ Ω) compared with that of the unbridged patterns ($R_{\text{unbridged}} = 120$ Ω). This is because the resistance of the bridged sample arises from two contributions, i.e., the CNT bridges and the Au

film. This result indicates that the CNT bridges provide a low-resistance electronic transport pathway between the SiO₂ patterns. The low resistance of the pattern-CNT-pattern units in our samples is consistent with the good contact between CNT tips and Au layers observed in Figure 2e, and the well-graphitized multi-walled tube structures.^[18]

In summary, we demonstrated the exclusive in-plane growth of CNTs in pre-defined directions and with tunable lengths by selective masking of SiO₂ patterns with a metal that does not catalyze nanotube growth. This method can be used to create nanotube bridges that interconnect SiO₂ patterns and provide low-resistance pathways for electrical transport. Similar strat-

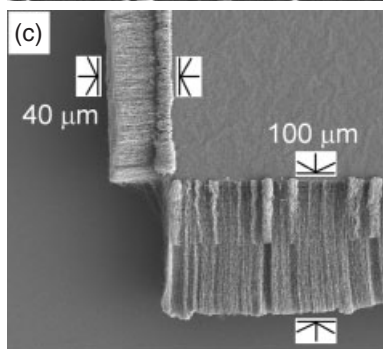
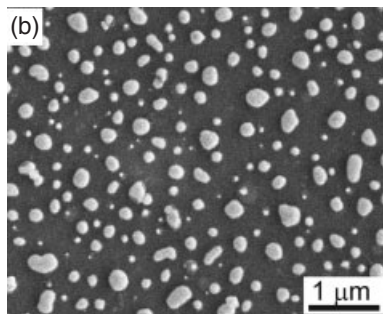
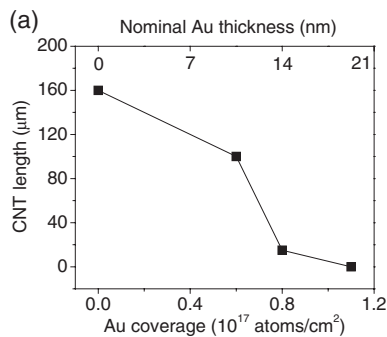


Fig. 3. a) CNT length plotted as a function of Au coverage on SiO₂. The nominal Au film thickness is also shown on the top axis. For all the cases, CVD conditions were identical and the reaction time was 30 min. b) SEM image of Au islands (white contrast) after annealing to 800 °C (the CVD temperature) on SiO₂ surface. c) CNTs grown from two side-walls of a SiO₂ template. Note the different CNT lengths: 40 μ m (left) and 100 μ m (down). The CNT lengths bear an inverse correlation with Au coverages of 0.75×10^{17} and 0.60×10^{17} atoms cm $^{-2}$, on the respective sidewalls, derived from the plot in Figure 3a.

gies that combine CVD with topographical masking of patterned substrates would be attractive for controllably growing nanotube–metal architectures for future devices for electronic switching, memory storage, sensing, and actuation.

Experimental

Arrays of 50 μ m \times 50 μ m silicon pillars were created on a Si wafer by coating and patterning a 1 μ m thick photoresist followed by deep etching of 30 μ m trenches using a plasmatherm tool. After stripping the resist, the wafer was heated to 1100 °C to form a 1 μ m thick SiO₂ layer by wet oxidation. This process results in 30 μ m high relief features with silica surfaces, as illustrated schematically in Figure 1a.

Au was sputtered onto SiO₂ substrates in a 50 mtorr Ar plasma at an anode voltage of 7 V and a current of 25 mA, leading to an average deposition rate of ~ 1 nm s $^{-1}$. Inside the sputter chamber, the substrates with SiO₂ patterns were placed in a near-vertical configuration, at a tilt angle of $\sim 20^\circ$, with a sample–cathode distance of 30 mm (Fig. 1b). This sample placement geometry results

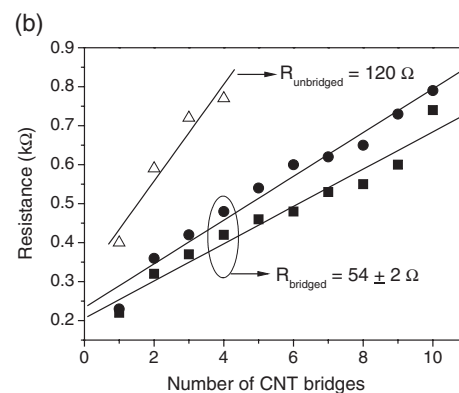
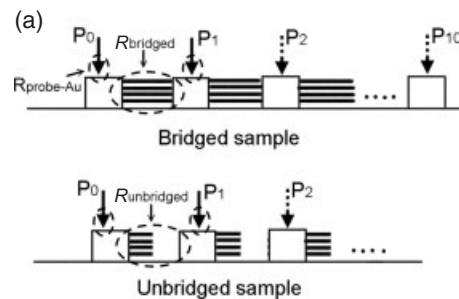


Fig. 4. a) A schematic sketch of configuration used to measure electrical resistance of Au-coated SiO₂ patterns with and without CNT bridges. The unbridged sample was prepared using a short CVD time so that CNTs did not grow long enough to connect adjacent SiO₂ patterns. During the measurements, one probe was fixed at P₀, while another probe was moved to different locations from P₁ to P₁₀, to record the resistances across different number of CNT bridges. b) Resistance plotted as a function of number of bridges. Circles and squares show the resistance behavior for structures with CNT bridges, while triangles show data obtained from unbridged structures. $R_{\text{unbridged}}$ is due to the Au layer sputtered on, and in between, the SiO₂ patterns as shown in the inset in Figure 2e.

in Au coverage on the top surface and one sidewall of each SiO₂ pattern that faces the Au flux, while the opposite sidewall is protected from Au coverage. Rutherford backscattering spectrometry (RBS) measurements carried out using a 2 MeV He⁺⁺ probe beam show that SiO₂ surfaces are covered with 1.1×10^{17} atoms cm $^{-2}$ of Au (nominal thickness of ~ 20 nm) when exposed to the Au sputter flux for 20 s.

The Au-coated SiO₂ patterns were placed into a tube furnace to grow CNTs selectively on SiO₂ surfaces without Au coverage by a CVD process using a xylene–ferrocene mixture [18,19]. For comparison, we also loaded substrates without Au coating in the CVD furnace. A solution of 0.4 g ferrocene dissolved in 40 mL xylene was fed into the CVD furnace at the temperature of 800 °C for time intervals ranging from 5 to 30 min. This method is well-known to produce aligned CNTs, which are typically multi-walled nanotubes with diameters of ~ 20 –50 nm [18].

Received: December 10, 2002
Final version: March 27, 2003

- [1] M. S. Dresselhaus, G. Dresselhaus, P. C. Eklund, *Science of Fullerenes and Carbon Nanotubes*, Academic Press, New York 1996.
- [2] J. W. Mintmire, B. I. Dunlap, C. T. White, *Phys. Rev. Lett.* **1992**, *68*, 631.
- [3] N. Hamada, S. Sawada, A. Oshiyama, *Phys. Rev. Lett.* **1992**, *68*, 1579.
- [4] L. A. Nagahara, I. Amiani, J. Lewenstein, R. K. Tsui, *Appl. Phys. Lett.* **2002**, *80*, 3826.
- [5] M. Burgard, G. Buesberg, G. Philipp, J. Muster, S. Roth, *Adv. Mater.* **1998**, *10*, 584.
- [6] Z. F. Ren, Z. P. Huang, J. W. Xu, J. H. Wang, P. Bush, M. P. Siegal, P. N. Provencio, *Science* **1998**, *282*, 1105.
- [7] S. Fan, M. G. Chapline, N. R. Franklin, T. W. Tomblor, A. M. Cassell, H. Dai, *Science* **1999**, *283*, 512.
- [8] A. Y. Cao, X. F. Zhang, C. L. Xu, J. Liang, D. H. Wu, X. H. Chen, B. Q. Wei, P. M. Ajayan, *Appl. Phys. Lett.* **2001**, *79*, 1252.
- [9] E. J. Bae, W. B. Choi, K. S. Jeong, J. U. Chu, G. S. Park, S. Song, I. K. Yoo, *Adv. Mater.* **2002**, *14*, 277.

- [10] N. R. Franklin, H. Dai, *Adv. Mater.* **2000**, *12*, 890.
 [11] N. R. Franklin, Q. Wang, T. W. Tomblor, A. Javey, M. Shim, H. Dai, *Appl. Phys. Lett.* **2002**, *81*, 913.
 [12] Y. Homma, Y. Kobayashi, T. Ogino, T. Yamashita, *Appl. Phys. Lett.* **2002**, *81*, 2261.
 [13] Y. Zhang, A. Chang, J. Cao, Q. Wang, W. Kim, Y. Li, N. Morris, E. Yenilmez, J. Kong, H. Dai, *Appl. Phys. Lett.* **2001**, *79*, 3155.
 [14] A. Ural, Y. Li, H. Dai, *Appl. Phys. Lett.* **2002**, *81*, 3464.
 [15] Z. J. Zhang, B. Q. Wei, G. Ramanath, P. M. Ajayan, *Appl. Phys. Lett.* **2000**, *77*, 3764.
 [16] B. Q. Wei, R. Vajtai, Y. Jung, J. Ward, R. Zhang, G. Ramanath, P. M. Ajayan, *Nature* **2002**, *416*, 495.
 [17] A. Y. Cao, X. F. Zhang, C. L. Xu, J. Liang, D. H. Wu, B. Q. Wei, *Appl. Surf. Sci.* **2001**, *181*, 234.
 [18] R. Andrews, D. Jacques, A. M. Rao, F. Derbyshire, D. Qian, X. Fan, E. C. Dickey, J. Chen, *Chem. Phys. Lett.* **1999**, *303*, 467.
 [19] C. N. R. Rao, R. Sen, B. C. Satishkumar, A. Govindaraj, *Chem. Commun.* **1998**, 1525.

Effects of Annealing on the Properties of Molecular Thin Film Heterostructures**

By Sandrine Heutz,* Georgeta Salvan, Tim S. Jones, and Dietrich R. T. Zahn

Optoelectronic devices based on organic thin film materials are looking increasingly attractive because of their low cost and high versatility. However to meet the demands of this emerging technology, ever more complex and controlled heterostructures have to be produced.^[1] An understanding of the basic properties of these complex heterostructures is crucial for optimizing device architectures and improving the resulting device performance.

Phthalocyanines (Pcs) and perylene (Pe) derivatives have been used in several types of organic thin film devices. They are particularly prominent in molecular solar cells,^[2] and devices based on these materials have resulted in some of the highest performances reported to date.^[3,4] Their single-layer characteristics have been investigated extensively, from epitaxial growth of very thin layers on semiconductor substrates,^[5,6] to unstrained growth of relatively thick layers on non-interacting substrates such as glass or indium tin oxide (ITO).^[1,7] H₂Pc and PTCDA both form crystalline films when deposited at room temperature on glass (or ITO) and adopt the well-known herringbone structure.^[8–11] Their arrangement with respect to the substrate is, however, different; the molecular planes of H₂Pc align perpendicular to the substrate,

whereas the PTCDA molecular plane lies parallel to it.^[9,10] Post-growth annealing of single-layer H₂Pc and PTCDA films has a significant effect on their properties. H₂Pc films display polymorphism provided the film thickness exceeds ~50 nm, where the metastable α phase which is obtained for deposition at room temperature transforms to a more stable β structure, which consists of a more compact herringbone arrangement.^[10,12–14] PTCDA also forms different polymorphs, α and β , but these have very similar lattice parameters.^[15] It has been reported that the α and β phases coexist when films are grown at room temperature on passivated Si(100) while a progressive transition to the α polymorph takes place at higher growth temperatures.^[16] We have recently established that for relatively thick (~10–150 nm) films deposited on glass substrates, only the α polymorph is obtained, independent of the growth conditions.^[17]

The growth of multilayer molecular thin film structures can lead to significant changes in the characteristics of the molecular film when compared to the single-layer film. It has been shown, for example, that the structural properties can be modified by the presence of an underlying ordered molecular layer.^[18,19] In the case of H₂Pc/PTCDA heterostructures, we have recently shown that when H₂Pc is deposited on top of a PTCDA first layer, it adopts a new templated structure in which the H₂Pc molecular planes are parallel to PTCDA, with an interplanar distance of 3.33 Å.^[20,21] Theoretical calculations show that this structural modification is a consequence of the intermolecular interactions at the heterointerface.^[22]

In this paper, we extend our work on the templated PTCDA/H₂Pc heterostructures and present a study of the effects of annealing on the structural, morphological and spectroscopic properties. Since it is known that H₂Pc single layers are sensitive to temperature treatment, we investigate the possible relaxation of the templated layered structure of H₂Pc on top of PTCDA. We then discuss how the stability of the individual layers is modified in a double-layer heterostructure. Our studies show that the templated H₂Pc structure is more stable than any of its known single-layer polymorphs and, furthermore, it can form a protective capping layer that prevents sublimation of PTCDA from the underlying layer.

Different in-situ annealing temperatures were applied to a PTCDA/H₂Pc heterostructure which was grown at room temperature by organic molecular beam deposition and consists of a 190 nm thick H₂Pc layer deposited on top of a 150 nm PTCDA layer. The X-ray diffraction (XRD) pattern of this heterostructure, Figure 1b, shows the main PTCDA peak at $2\theta = 27.6^\circ$, which corresponds to diffraction from the (102) planes and an interplanar spacing of 3.22 Å. This peak is characteristic of single-layer PTCDA films as can be seen from the corresponding diffraction scan for a 150 nm thick PTCDA film in Figure 1a.^[17] The shoulder in Figure 1b centered at 26.8° is characteristic of the planar H₂Pc templated structure, with an interplanar (and intermolecular) spacing $d = 3.33$ Å.^[20,21] No changes can be seen in the XRD patterns after annealing to 200 °C.

High annealing temperatures (~325 °C) are known to induce the $\alpha \rightarrow \beta$ phase transition in H₂Pc single layers, followed

[*] Dr. S. Heutz, Prof. T. S. Jones
 Centre for Electronic Materials and Devices
 Department of Chemistry, Imperial College London
 London SW7 2AZ (UK)
 E-mail: sheutz@ic.ac.uk

Dr. G. Salvan, Prof. D. R. T. Zahn
 Halbleiterphysik, Technische Universität Chemnitz
 Reichenhainerstraße 70/644, D-09107 Chemnitz (Germany)

** The authors gratefully acknowledge the Marie Curie Training Site "Carbon Containing Thin Films" for funding of the collaboration with T. U. Chemnitz, and wish to thank Axel Fechner for technical assistance. S. H. thanks the department of Chemistry, Imperial College, for provision of a teaching assistantship, and G. S. acknowledges the EU funded Human Potential Research Training Network DIODE (Contract No.: HPRN-CT-1999-00164) for financial support.